

Transient Raman Snapshots of the Twisted Intramolecular Charge Transfer State

*Shreetama Karmakar^a, Abhinandan Ambastha^a, Ajay Jha^{a,b}, Aditya Dharmadhikari^c, Jayashree Dharmadhikari^d, Ravindra Venkatramani^a, and Jyotishman Dasgupta^{*a}*

AUTHOR ADDRESS

^a Department of Chemical Sciences, Tata Institute of Fundamental Research, Mumbai 400005, India

^b Max Planck Institute for the Structure and Dynamics of Matter, Hamburg, Germany

^c Department of Nuclear and Atomic Physics, Tata Institute of Fundamental Research, Mumbai 400005, India

^d Raman Research Institute, Sadashivnagar, Bangalore 560 080, India

Supporting information

Contents

SECTION 1: MATERIALS AND METHODS	4
SECTION 2: CHARACTERIZATION.....	7
Figure S1:	7
Figure S3	9
Figure S4	9
Table ST1	9
SECTION 3: SUPPLEMENTARY TRANSIENT ABSORPTION DATA.....	10
Figure S5a	10
Figure S5b	10
Figure S5c	11
Figure S5d	11
Figure S5e	12
Figure S5f.....	12
.....	13
Figure S5g: a) Transient Absorption spectra of 1mM DEST in ethylene glycol with 490 nm pumping in the visible (pump power = 10 nJ) and NIR (power = 0.2 μ J) regions. b) Kinetic traces of time constant at 620 nm SE and c) 910 nm ESA. Red dots represent experimental data and the maroon lines shows the multi-exponential fits.	14
.....	15
Figure S5i	15
Figure S6a	16
Figure S6b	17
Figure S6c	18
Figure S6d.....	18
Figure S6e	19
Figure S6f.....	20
SECTION 5: OPTIMIZATION OF GEOMETRY IN S_0 AND S_1 AND CALCULATION OF VIBRATIONAL FREQUENCY METHODOLOGY	22
SECTION 6: EVALUATING THE STRUCTURE AND PROPERTIES OF S_0 AND S_1 / TICT STATE OF DEST USING DIFFERENT SOLVENTS AND MODELS IN THE DFT/CAM-B3LYP LEVEL	24
Figure S7	24
Figure S8	27
Table ST5	28

Figure S9	29
Table ST6:	30
Figure S10	31
Table ST7	32
Figure S11	34
Figure S12	35
Table ST8:	36
Table ST9:	37
Figure S13	Error! Bookmark not defined.
References	39

SECTION 1: MATERIALS AND METHODS

Sample Synthesis and Purification. Synthesis of DEST was carried out by refluxing equimolar quantities of 4-picoline (0.97 ml) and 1.5 ml of methyl p-toluenesulfonate for two hours. 1.49 g of 4, 4-diethyl aminobenzaldehyde, and 0.2 ml of piperidine was added to the mixture and refluxed for 4 hours. This refluxed solution mixture was poured into 200 ml of diethyl ether to yield DEST.¹ The product was purified using HPLC (Shimadzu Prominence LC 20A) by varying the solvent from 5% acetonitrile in water to 95% in 65 minutes. The eluent collected between 25-27 minutes was pure cation of DEST. The sample was characterized before and after purification by NMR (Figure S1) using a VARIAN-600 MHz spectrometer.

Steady State Spectroscopic Measurements. Steady-state absorption was recorded in a (Jasco UV-VIS V670) spectrophotometer for 10 μ M solution of DEST in water, methanol, and ethylene glycol. Emission and excitation spectra at 600 nm for the same solution (Figure S2) were collected using a fluorimeter (SPEX Fluorolog model 1681T).

Ultrafast Time-Resolved Spectroscopy. For the ultrafast pump-probe measurements, the sample solution was taken in a 2 mm thick flow cuvette, and the solution was circulated continuously by a peristaltic pump throughout the measurement to minimize sample damage.

a) Transient Absorption (TA) Measurements. The details of the ultrafast transient absorption set-up have been described previously.^{2,3} Briefly, a 4 - 4.8 nJ output beam of a Ti-Sapphire oscillator (80 MHz repetition rate, 25 fs, 800 nm, 100 nm bandwidth at FWHM from Coherent Mira-5) was amplified by a regenerative amplifier (30 fs, 800 nm, 65 nm bandwidth at FWHM, Coherent Legend Elite USX 1k) to 3.5 mJ/pulse.

The resulting beam was split using a 50:50 beam splitter. One part of the beam was passed through an optical parametric amplifier (Coherent Opera Solo) to generate the actinic pump (bandwidth \pm 10-15 nm), which was attenuated to 100 - 500 nJ. A portion of the other part of the beam was focussed on a 2 mm

thick sapphire plate to generate a white light continuum probe 450 - 1600 nm. The delay between pump and probe was provided by a motorized translation stage (Newport) outfitted with a quadra-pass mirror assembly. The IRF was measured to be ~ 90 fs from the measurement of the optical Kerr effect. The sample solution was circulated inside a flow cell throughout the measurement using a peristaltic pump. The probe was detected by a multichannel detector procured from Ultrafast Systems, Sarasota, FL, and it was visualized using Helios software. The recorded data were processed with Surface Explorer software. The kinetic data were fitted with 2 or 3 exponential rise and decay functions convoluted with the IRF using IGOR 5 PRO software with home written codes.

b) Femtosecond Stimulated Raman (FSRS) Measurements. The details of the FSRS set-up have been discussed elsewhere.^{3,4} FSRS technique requires the overlap of three beams: a broadband femtosecond probe, a femtosecond actinic pump, and a narrowband picosecond Raman pump. The same actinic pump pulse as in TA measurement was used for the FSRS measurements. For the generation of the other two pulses, a second beam splitter in the path of the probe beam was used to split the beam into two. One part was used to generate a compressed white light probe pulse in the NIR region. The probe was generated in the same way as described for TA measurement. A long-pass filter was used to take out the NIR part of the white light, which was compressed using a prism compressor to minimize group velocity dispersion.

The second portion of the femtosecond beam was used to generate the Raman pulse. The broadband pulse was dispersed using a grating, and a portion of the dispersed beam was selected at the focal plane through a narrow slit (4f-grating filter) while subsequently compressing it to a picosecond pulse.³ The position and width of the slit can be varied to choose a particular wavelength (in the 790-830 nm region) and energy of the pulse, respectively. However, the slit-width also determined the resolution of the signal. Throughout the experiment, the slit width was maintained to obtain a resolution of 20 cm^{-1} while the time-resolution was ~ 70 fs. An integrated CCD detector with a triple grating monochromator ACTON AP 2300 (Princeton Instruments) was used as the detector, and a homemade program in LabVIEW was used for visualizing and recording the data. For further discussion on the processing of FSRS data, please refer to the Supporting Information (Section 4).

Computational methods.

To predict the structure of the TICT state, DFT and TDDFT electronic structure calculations at the CAM-B3LYP/6-31+G (d) level have been performed (see Supporting Information sections 5 and 6 for details). The CAM-B3LYP functional is a range-separated hybrid that includes a distance-dependent mixing Hartree-Fock exchange and Becke 1988 exchange with the hybrid B3LYP exchange-correlation functional to provide an improved description of CT transitions and states. The geometry of the DEST cation was optimized using Gaussian 2009 package program.⁵ The ground state geometry was optimized, and Raman frequency modes for S_0 were calculated using the DFT level of theory with a 6-31G+ basis set with CAM-B3LYP functional. Optimization and frequency calculation of the S_1 state has been done using TDDFT theory on the same basis set and functional as of the ground state. However, Gaussian 09 lacks any method to predict Raman activities of the S_1 state in the TDDFT level of calculation. To account for the solvation effect, we have used different solvation models using water and methanol as solvent. The polarizable continuum model was used as a preliminary step to understand the effects of the solvent (methanol, water) on the energetics, geometries, and extent of charge transfer in the cation. Since the latter model was unable to capture the steady-state and transient spectral features consistently, explicit solvation models were used by adding water molecules to the gas phase structure. The molecular orbitals were visualized in GaussView 5.0 software for the ground state to local excited state transition and the vertical transition in TICT manifold by generating cube files using the checkpoint files of geometry optimization calculations. Single point energy calculations from the S_0 optimized structures to the corresponding first excited states were used as estimated Franck-Condon transition energies.

SECTION 2: CHARACTERIZATION

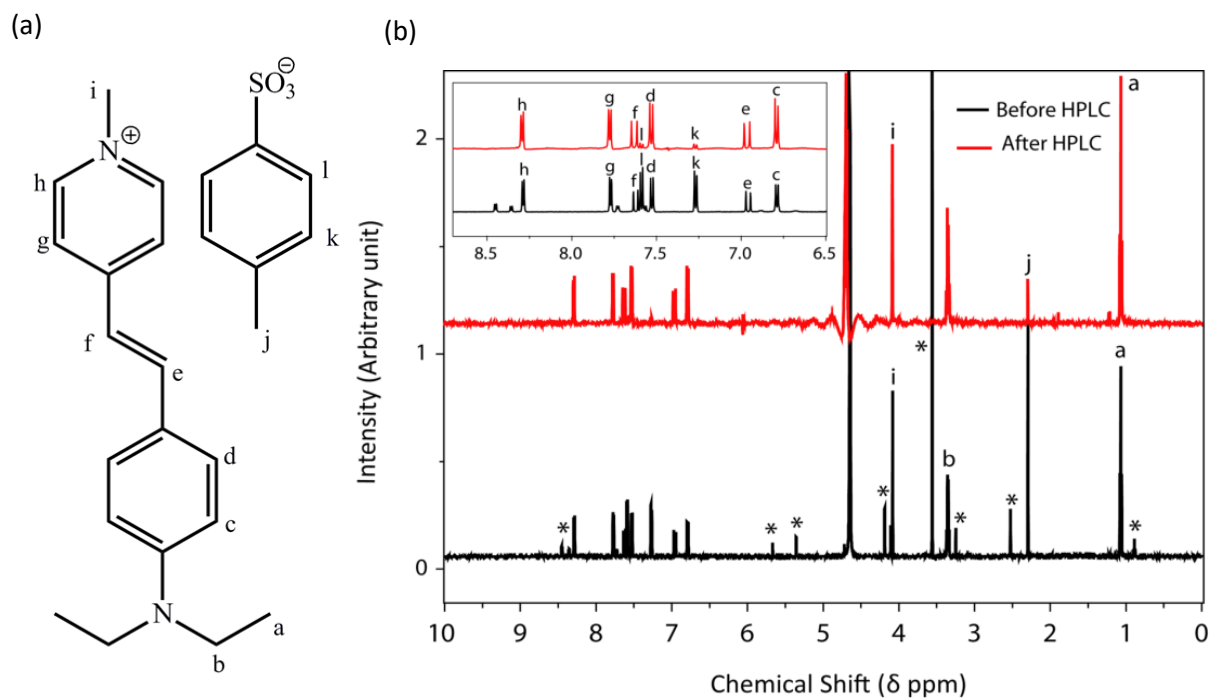


Figure S1: a) NMR assignments of DEST protons and b) NMR spectra of 1mM DEST in D₂O before HPLC and 0.5 mM DEST in D₂O after HPLC. The aromatic region is magnified in the inset. Peaks from the tosylate anion (j, k, and l) diminish after HPLC presumably due to exchange with trifluoroacetate anion. Figure S1(b) clearly shows that the impurity peaks (marked by asterisks) in the lower panel (black trace) go down almost completely in the HPLC purified sample (red trace).

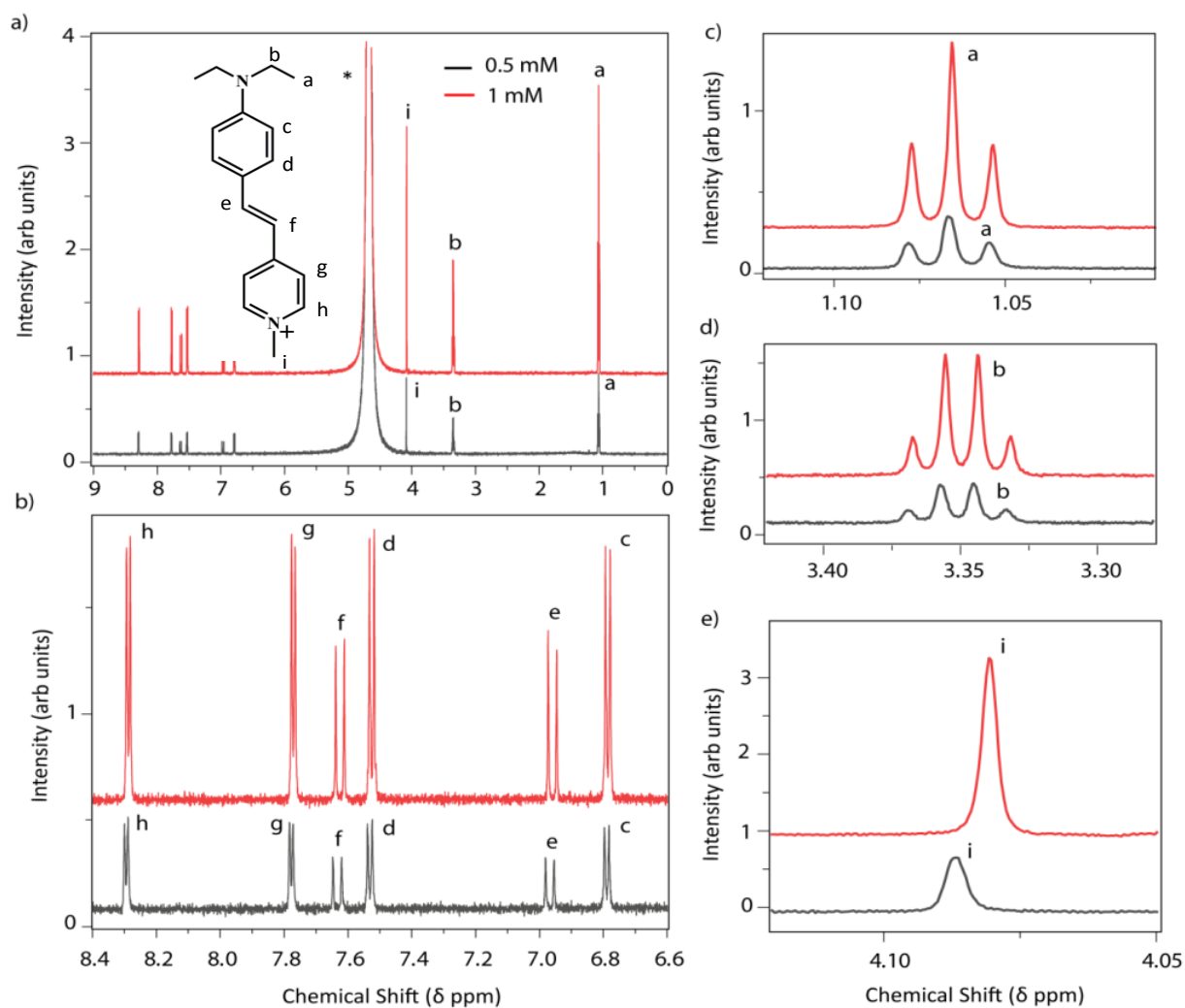


Figure S2: NMR spectra of the cation of DEST in a VARIAN-600 MHz (inset, with iodide as a counter anion) a) total no. of peaks, b) aromatic and ethylenic peaks, c), d) and e) aliphatic peaks. Spectra recorded for 0.5 mM, and 1mM solution of DEST cation does not show any additional peaks. The slight upfield shift of < 0.01 ppm in some peaks upon an increase in concentration is within calibration error. This data shows that there is no observable aggregation, and most of the population remains monomeric.

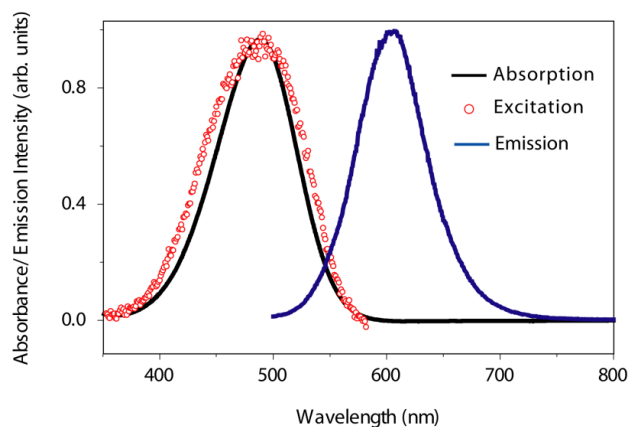


Figure S3: Absorption, emission, and excitation spectra of 10 μM DEST in methanol. The emission was collected subsequent to excitation at 490 nm.

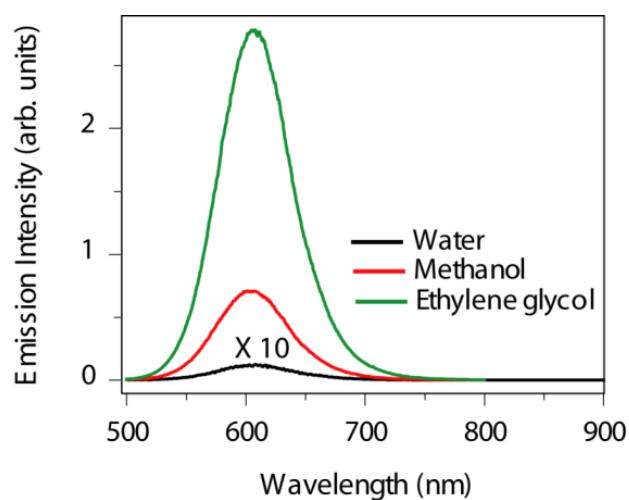


Figure S4: Relative emission intensities of DEST in different solvents. The emission intensity in water has been multiplied by a factor of 10 for visibility. The concentrations of DEST chosen in all three solvents were the same, i.e., 10 μM .

Table ST1: Physical constants of the solvents

Solvents	Dielectric constant (At 20° C) ⁶
Water	80.2
Methanol	32.7
Ethylene Glycol	37.7

SECTION 3: SUPPLEMENTARY TRANSIENT ABSORPTION DATA

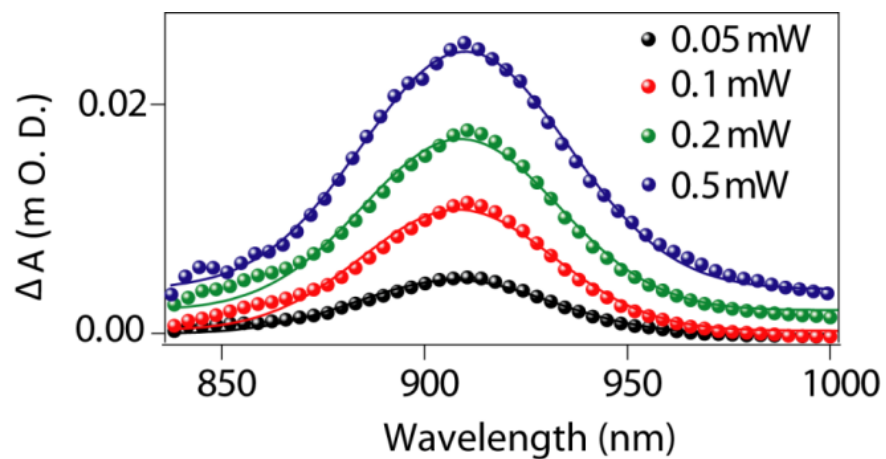


Figure S5a: Power dependence from 0.05 to 0.5 mW (50-500 nJ for 1000 s^{-1} pulse repetition rate) of the NIR feature at time delay ($\sim 1 \text{ ps}$) of DEST at 910 nm with Gaussian fits to calculate the area under the curve (solvent: methanol).

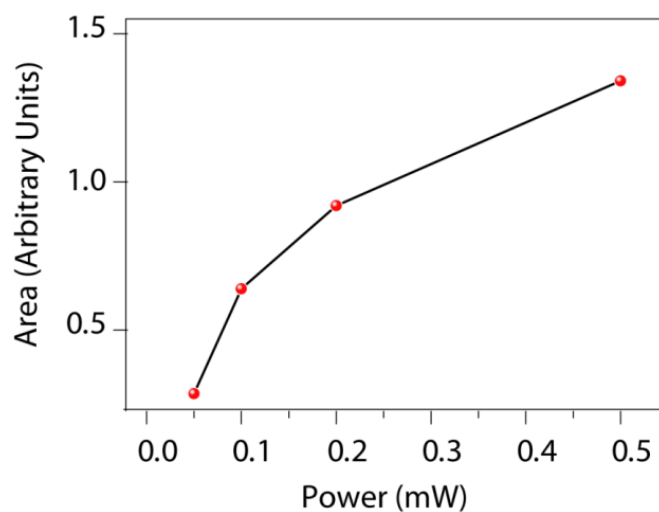


Figure S5b: Power dependence of the fitted area under the NIR feature of DEST in methanol at 910 nm.

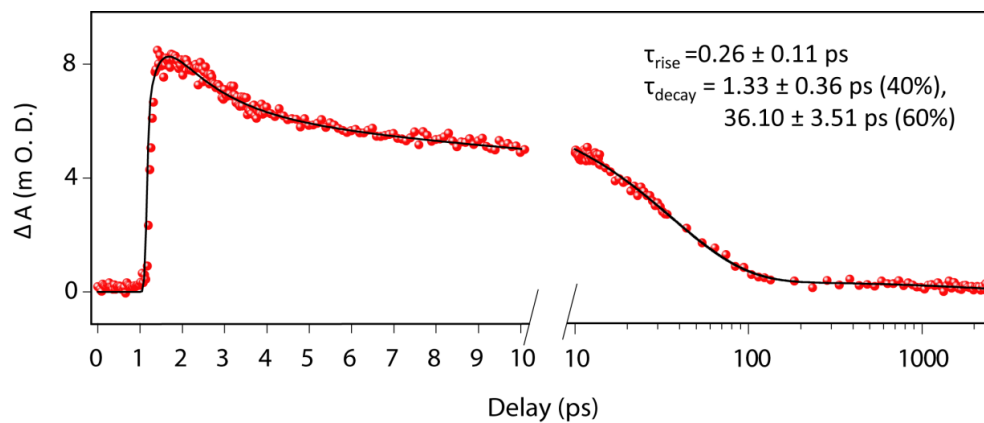


Figure S5c: Kinetics of the NIR feature of DEST at 910 nm at 50 nJ power of the actinic pump (solvent: methanol).

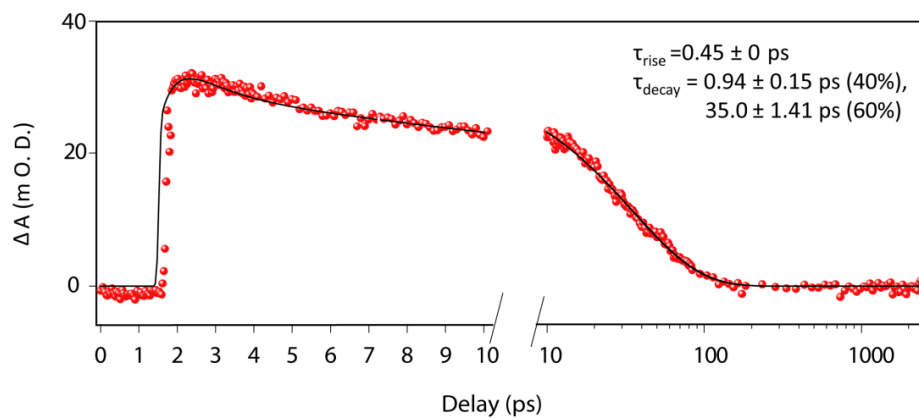


Figure S5d: Kinetics of the NIR feature of DEST at 910 nm at 400 nJ power of the actinic pump (solvent: methanol).

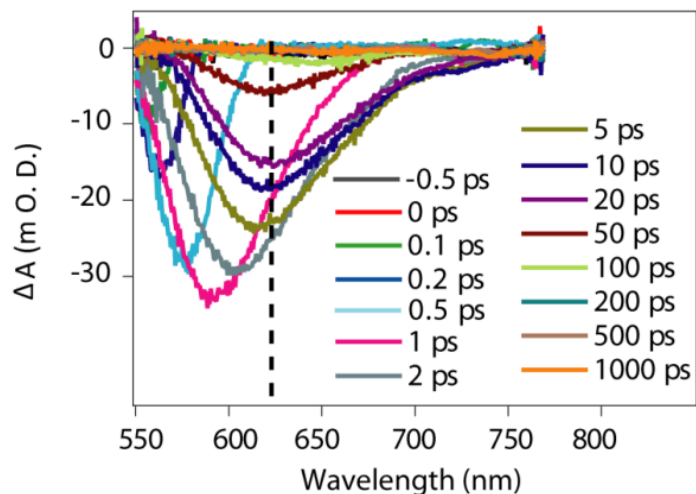


Figure S5e: TA spectra of 1mM DEST in methanol (refer to Figure 2, the main manuscript) before chirp correction for group velocity dispersion. Actinic pump (490 nm) power = 10 nJ.

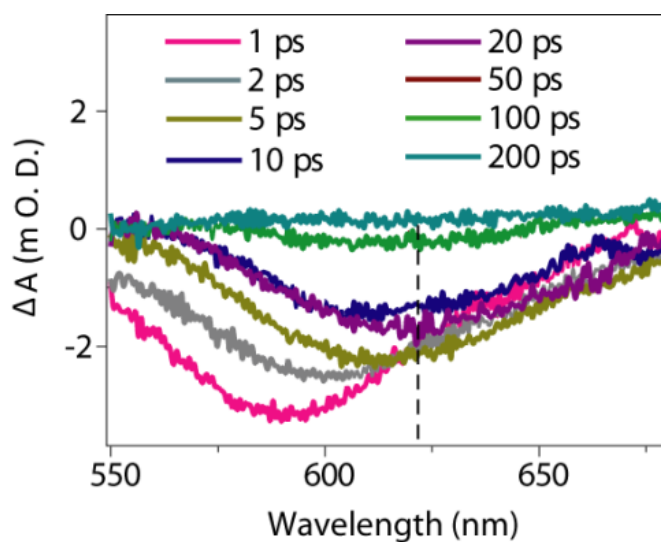


Figure S5f: TA spectra of 10 μ M DEST in methanol indicates a similar spectral profile and dynamic shift of the SE (refer to Figure 2, the main manuscript). Actinic pump (490 nm) power = 1 μ J.

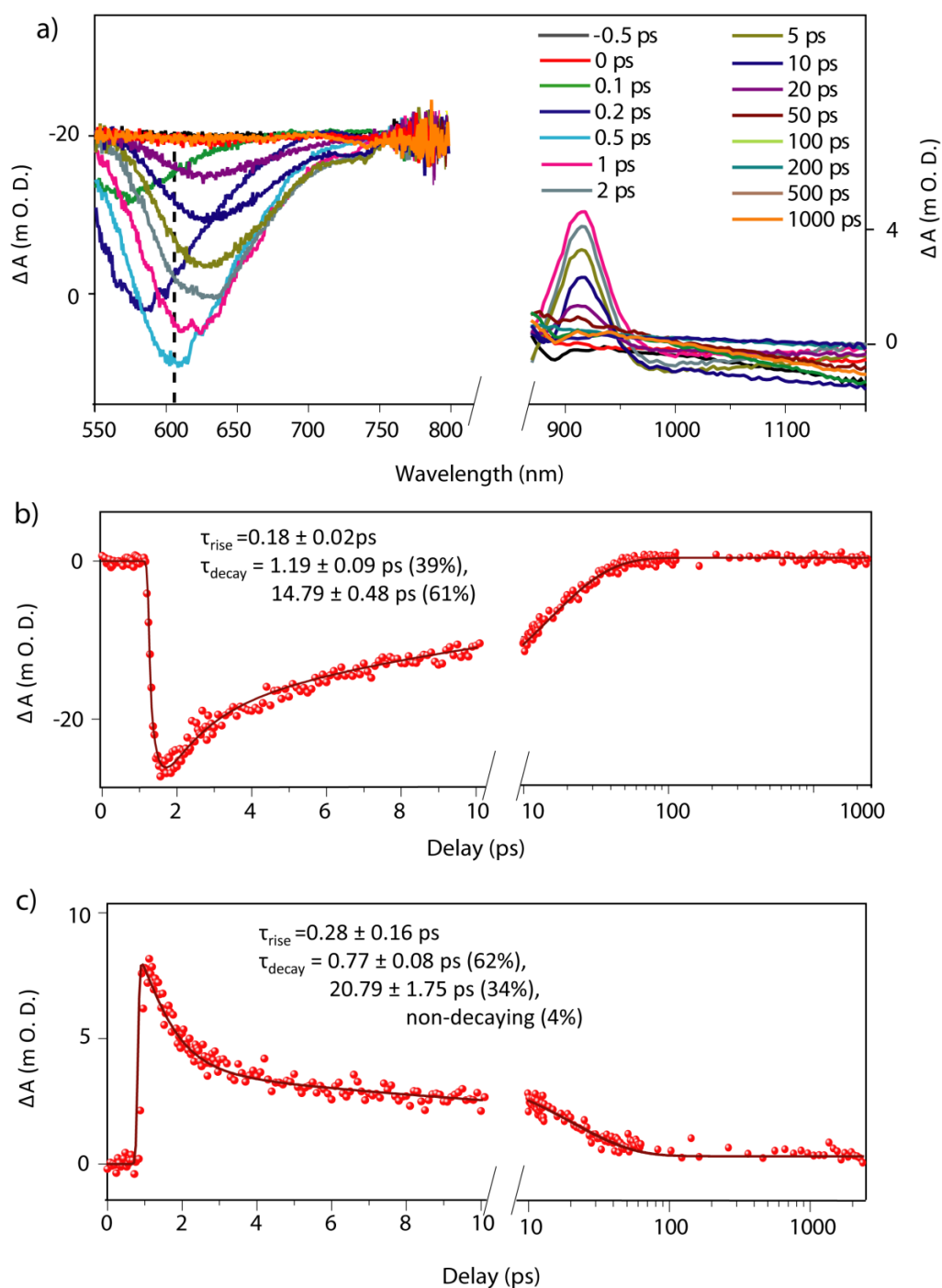


Figure S5g: a) Transient Absorption spectra of 1mM DEST in water with 490 nm pumping in the visible (pump power = 10 nJ) and NIR (power = 0.2 μJ) regions. b) Kinetic traces of time constant at 620 nm SE and c) 910 nm ESA. Red dots represent experimental data, and the maroon lines show the multi-exponential fits.

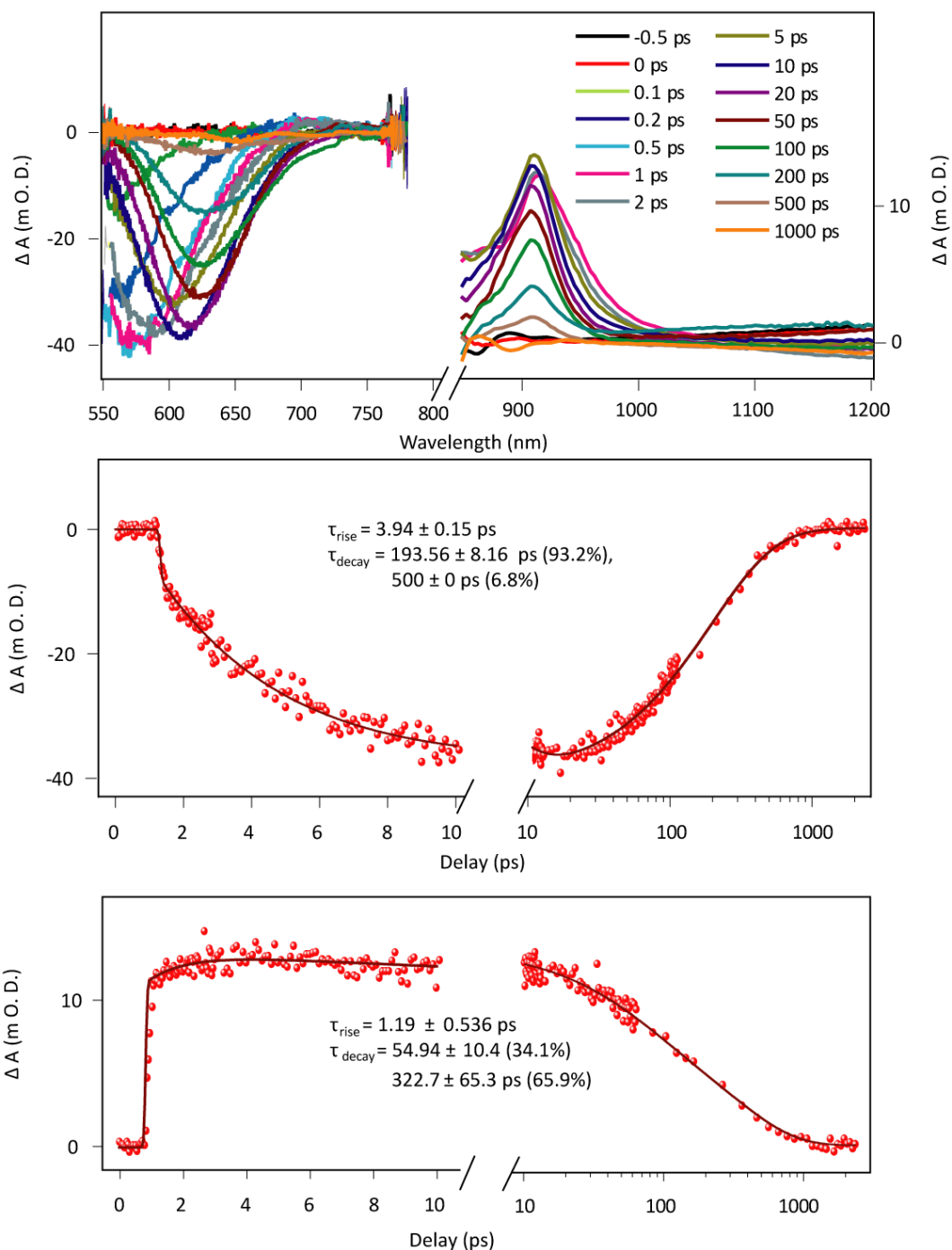


Figure S5h: a) Transient Absorption spectra of 1mM DEST in ethylene glycol with 490 nm pumping in the visible (pump power = 10 nJ) and NIR (power = 0.2 μ J) regions. b) Kinetic traces of time constant at 620 nm SE and c) 910 nm ESA. Red dots represent experimental data, and the maroon lines show the multi-exponential fits.

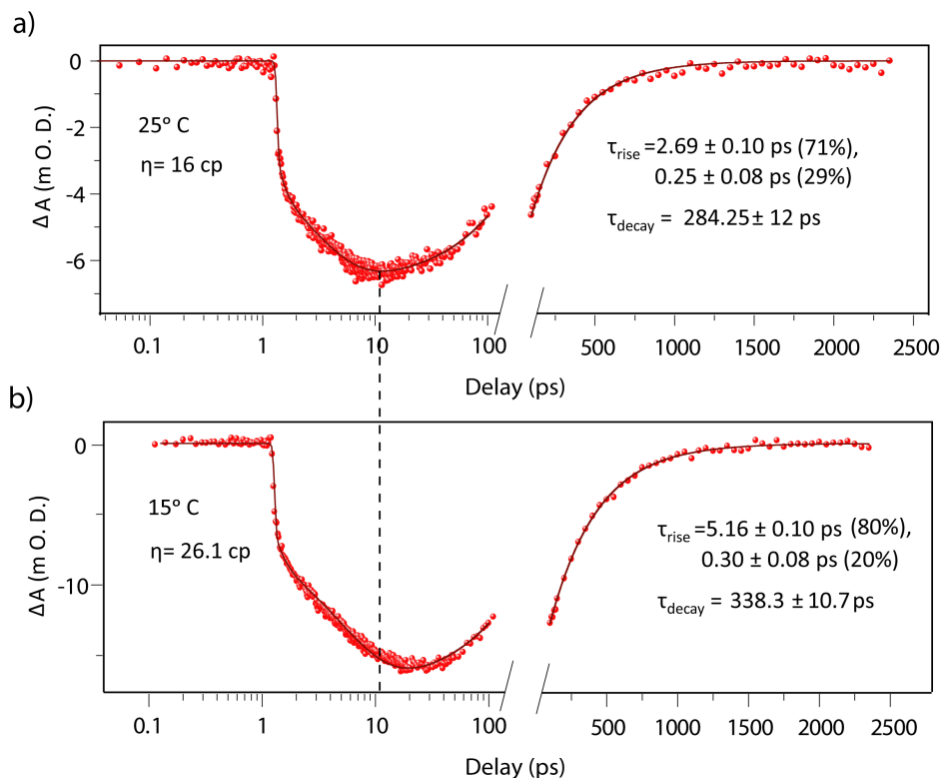


Figure S5i: Kinetics of 620 nm stimulated emission of DEST in ethylene glycol data at two different temperatures. Viscosities of the solvent change from 16 cp at 25°C to 26.1 cp at 15°C.⁷

SECTION 4: PROCESSING OF FSRs DATA

For the detection of the FSRs signal, it is necessary to have both the Raman pump and probe beams overlapped spatially and temporally in the sample. The chopper is kept in the path of the Raman beam, and the stimulated Raman signal is detected as the log of the ratio $I_{(\text{Raman+probe})} / I_{\text{probe}}$. To obtain the excited state signal, we need to measure the stimulated Raman in the presence and absence of the actinic pulse, respectively. We refer to the dataset in the presence of actinic pulse at various pump-probe delays ‘ON’ data and that in the absence of actinic pump as ‘OFF’ data (refer to Figure S4a), whereas, putting the chopper in the path of the actinic pump (with the Raman pump turned off) enables us to measure the transient absorption (‘TA’) features at different time delays. The ‘OFF’ data is averaged, baseline

corrected, and fitted using the IGOR 5 PRO software to obtain a noise-free simulation of the ground state stimulated Raman spectrum. Multiple sets of raw ‘ON’ data were collected at each pump-probe delay, and 10 data points were averaged to get a single ‘ON’ spectrum. Also, the ‘OFF’ data were collected frequently during the experiment to monitor any change in the probe spectrum with time. In the current work, an excited-state peak at 1650 cm^{-1} appeared well separated from the ground state features. So, we compensated the background of the raw ‘ON’ signals by subtracting the ‘TA’ feature from it and used the resulting data (Figure S4c) to calculate areas under that peak and the absolute values of the Raman shift as different pump-probe delays. For the final processing of the data, we first obtained raw ‘ON-OFF’ spectra, bleach-filled it with the simulated ground state spectrum, and baseline corrected the bleach-filled spectra to obtain baseline-free excited state spectra. See Figure S6b-e for more details.

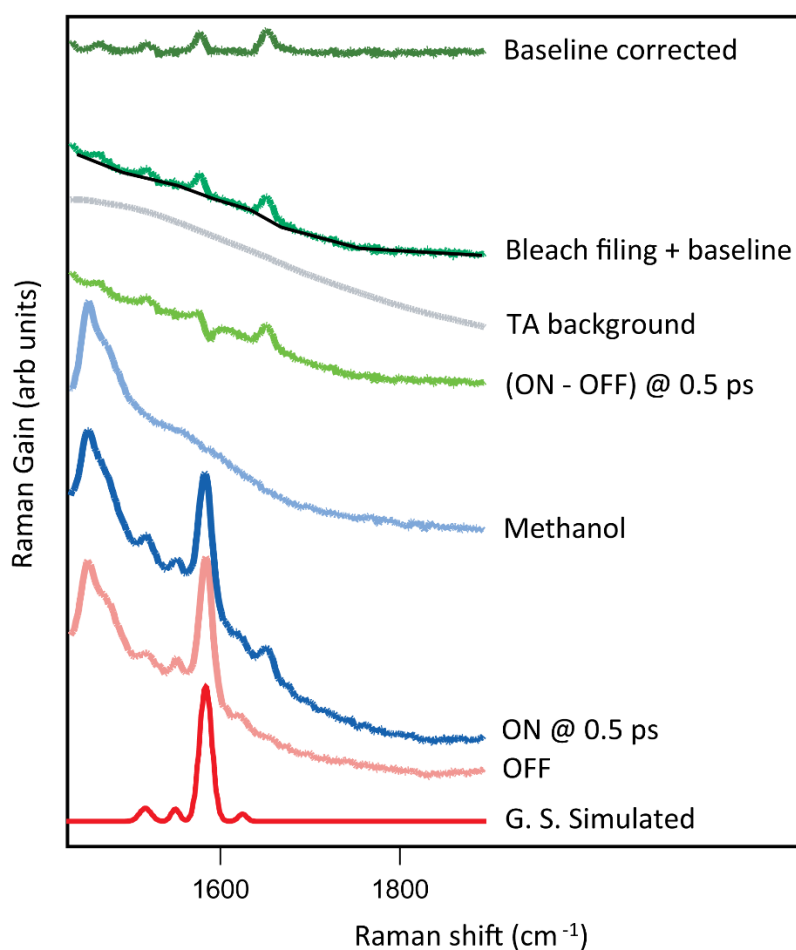


Figure S6a: Processing sequence of FSRS spectra at a pump-probe delay of 0.5 ps; from bottom to top:

Simulated Ground state stimulated Raman (red) after averaging the ‘OFF’ spectrum (pink), baseline corrected and fitted with IGOR PRO 5; The ‘ON’ spectrum at 0.5 ps pump-probe delay clearly shows the 1650 cm^{-1} mode. The peak at 1500 cm^{-1} arises from the solvent (methanol, steel blue). The raw ‘ON-OFF’ spectrum (light green) shows the excited state peaks as well as the ground state bleaches; after the addition of a fraction of the ground state simulated Raman, the bleaches are filled (darker green). A baseline (black), having similar curvature as that of the TA’s response (gray), is drawn. Finally, the topmost trace (darkest green) shows the baseline subtracted, bleach filled spectrum representative of pure excited state spectrum, at a pump-probe delay of 0.5 ps.

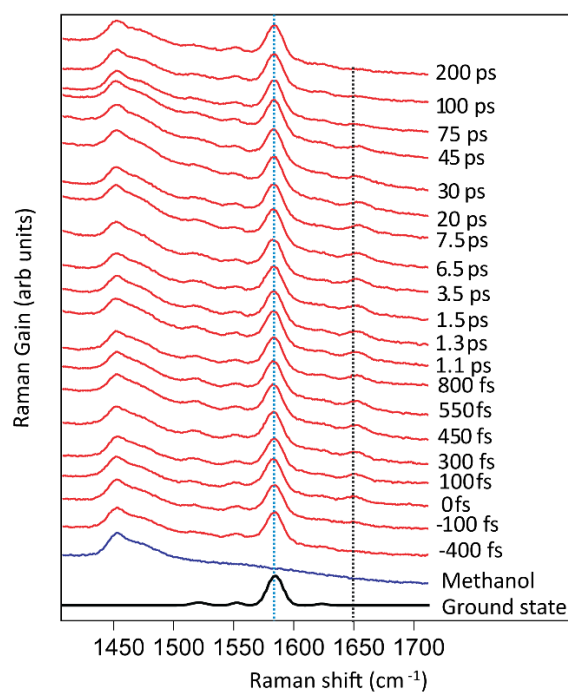


Figure S6b: Temporal evolution of ‘ON’ spectra after subtracting the raw TA background (gray line, Figure S5a). A manually drawn baseline would take care of the sloping background.

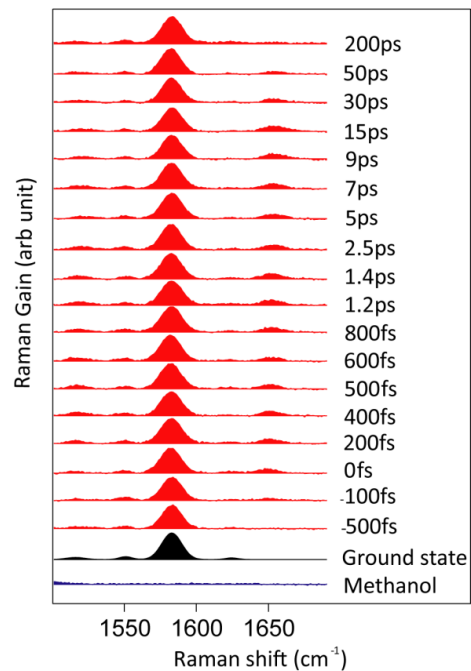


Figure S6c: Temporal evolution of 'ON' spectra after subtraction of a manually drawn baseline.

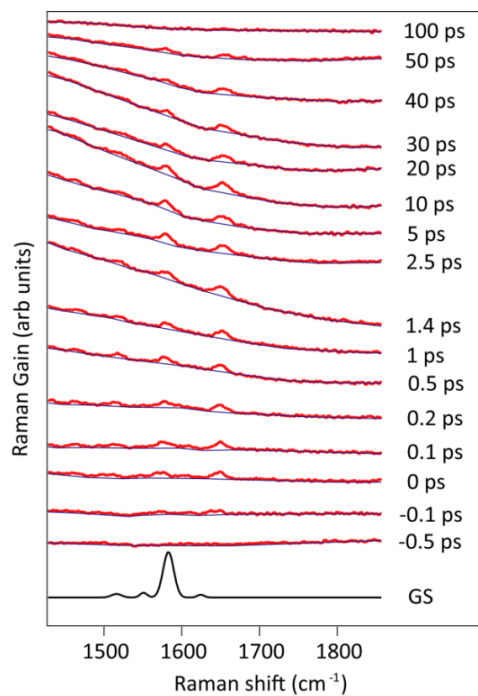


Figure S6d: Baseline corrections (in thin black lines) for the bleach-filled 'ON-OFF' spectra (red) at different pump-probe delays.

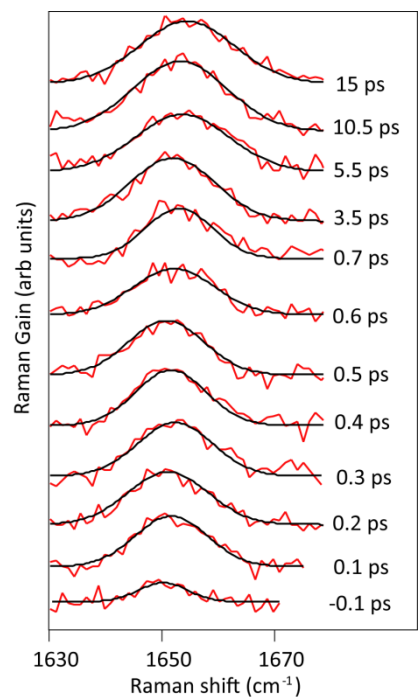


Figure S6e: Gaussian fits of the area under the 1650 cm⁻¹ mode at different pump-probe delays show the change in area as well as the shift in peak maximum.

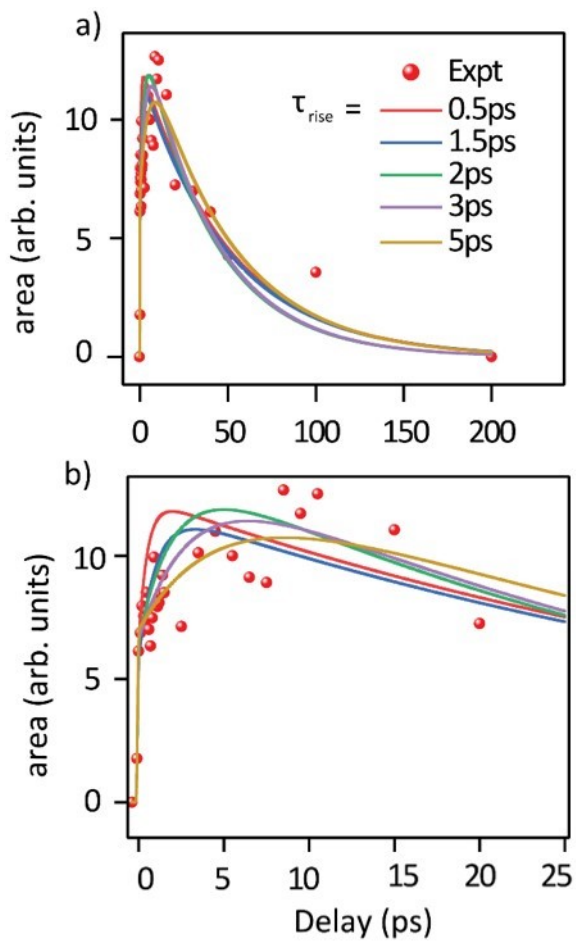


Figure S6f: Kinetic fits of the FSRS dynamics with varying parameter space for an exponential model: (Top) The overall plot (from 0-250 ps) for integrated the area under the 1650 cm^{-1} peak for DEST in methanol with different rise times varying from 0.5 to 5 ps although with fixed decay times. (Bottom) Expanded range of the same plot from 0-25 ps clearly showing the quality of fits to capture the rise times.

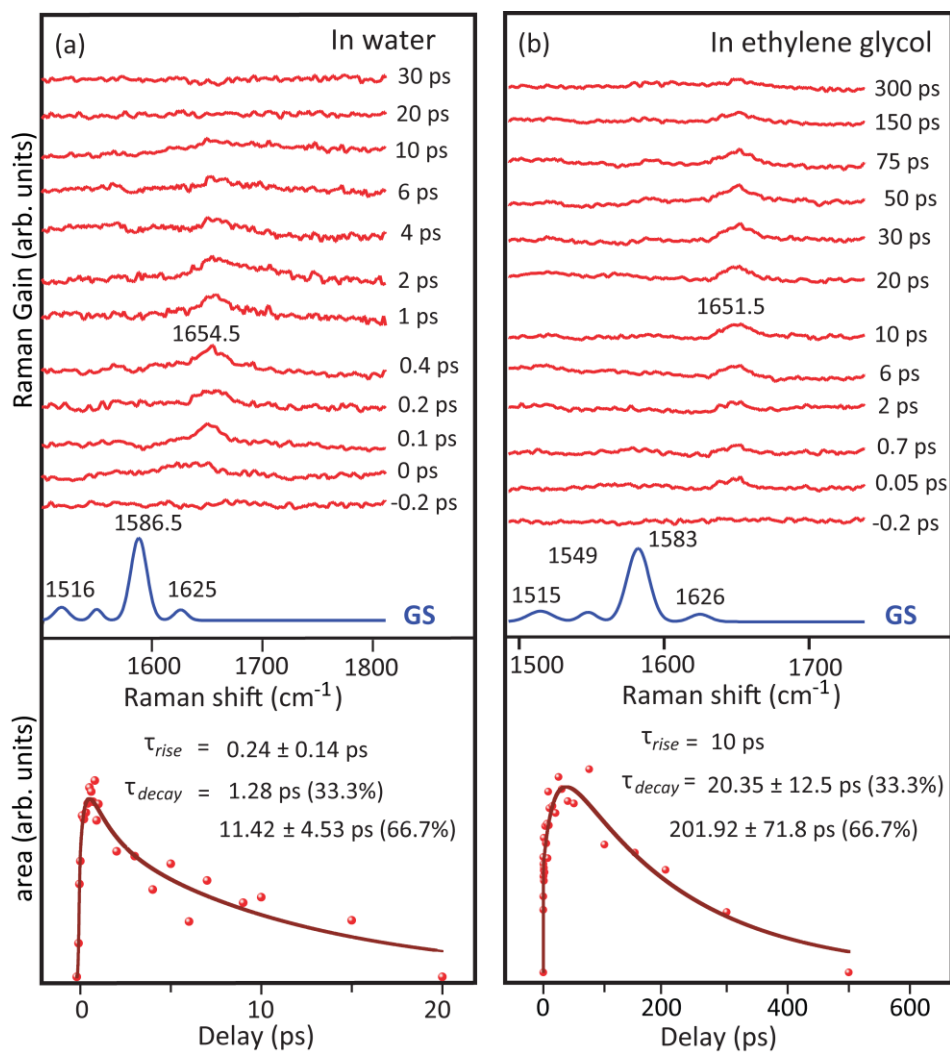


Figure S6g: FSRS of 1 mM DEST in (a) water and, (b) ethylene glycol. The kinetics of area under the 1654.5 and 1651.5 cm^{-1} peaks for water and ethylene glycol, respectively, are shown in the bottom of each panel.

SECTION 5: OPTIMIZATION OF GEOMETRY IN S_0 AND S_1 AND CALCULATION OF VIBRATIONAL FREQUENCY METHODOLOGY

The geometry optimization and frequency calculations were performed, keeping in mind the following caveats and limitations of the methodology and models used:

- i. Different calculation methodologies (i.e. HF, DFT/B3LYP, DFT/CAM-B3LYP, MP2 or CCSD) are known to have a different extent of systematic errors with respect to the experimentally obtained energetics and spectral data (e.g. UV-VIS and vibrational frequencies). In combination with different levels of calculations (i.e. different basis set), these methods are known to exhibit differences in accuracies which are well documented in the literature.^{8,9}
- ii. Differences in the methodologies and levels of calculation may result in significant differences in the optimized geometries in the ground as well as the excited state.
- iii. The systems/ models considered for the calculation may affect the accuracy of the agreement with the experimental data and the model of a chemical/excited state process.

Here we selected DFT/CAM-B3LYP method since the system has electron donor-acceptor groups, and the electronic transitions may have significant charge transfer characteristics, along with further charge separation in the CT manifold. In particular, the range-separated hybrid CAM-B3LYP functional is useful in describing the electronic transitions and energetics of charge transfer transitions and states¹⁰.

In our small molecular system, the use of conventional DFT method, which lacks the description of long-range dispersive interaction¹¹ was appropriate since intermolecular stacking interactions are not present. The choice of basis set 6-31+G (d) was made keeping in mind the optimization of calculation time with the accuracy of the final geometry, energetics, and spectra. With this choice of method and basis set, the reported agreements between experimental and theoretical spectral data (IR/Raman) for several molecular systems are found to be reasonable and can be improved using a particular scaling factor.⁶ Therefore, we used appropriate scaling factors for the vibrational frequencies whenever necessary.

The geometry optimizations were carefully done. Since the system is a conjugated aromatic system, we started with a planar ground state geometry, and this is also in accordance with the calculations done by

other groups on similar cations⁶. The optimization to a minimum was confirmed from the absence of any imaginary normal mode frequency for all the optimized structures. While optimizing the S₁ state geometry, we were taking care to check all the possible twisted structures as the starting geometry. Incidentally, for each model, a single stable minimum was found.

Afterwards, we experimented with different models of explicit solvation and came up with a model that has the best agreement with all the experimental data. The explicit solvation model was built with water molecules at specific sites (Figures S9- S13 and Tables ST6 – ST9) in addition to the gas-phase structure of DEST cation. The resulting structures and their spectral properties were subjected to rigorous comparison with experimentally obtained values, e.g. absorption spectrum of the cation, Raman spectrum in the ground and excited state. Also, the feasibility of a large structural change (i.e. the TICT model) was given utmost importance based on the pump-probe TA data. Thus, we conclude that the use of explicit solvent models, e.g. hydrogen bonding interaction may be required to model the TICT state, its vibrational modes and its formation timescales in different solvents.

SECTION 6: EVALUATING THE STRUCTURE AND PROPERTIES OF S_0 AND S_1 / TICT STATE OF DEST USING DIFFERENT SOLVENTS AND MODELS IN THE DFT/CAM-B3LYP LEVEL

Different models and structures were taken as a starting point for a thorough evaluation of the TICT structure of DEST in solvents, since the structure and properties of the ground, as well as TICT state, may be quite different in solvent environments compared to the gas phase description.

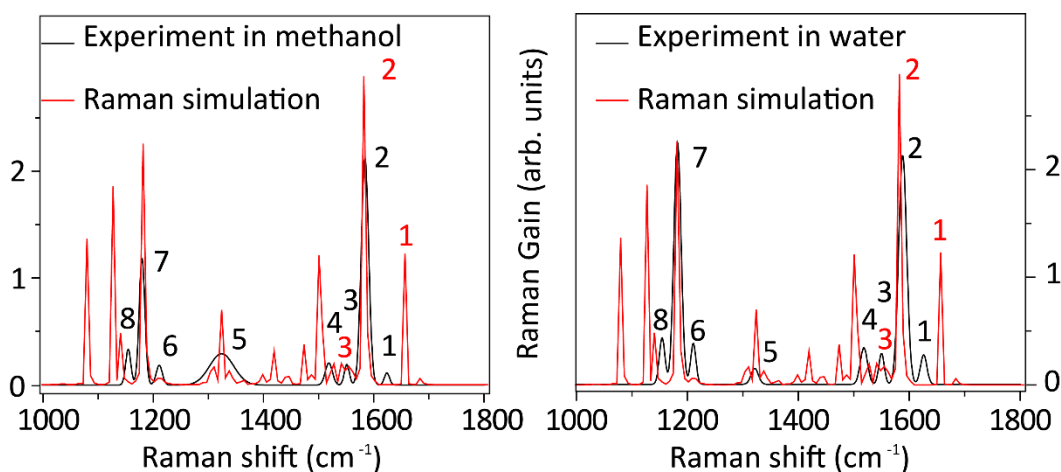


Figure S7: Comparison between experimentally obtained ground state Raman frequencies of DEST in methanol (left panel, black trace) and water (right panel, black trace) and the calculated Raman frequencies (red traces) in the CAM-B3LYP/6-31+G* level of theory for vacuum. A scaling factor of 0.97 has been used for the calculated frequency values. The modes marked as 1-3 in red are described in Table ST3.

Table ST2: Structural parameters of the optimized S_0 and S_1 in CAM-B3LYP/6-31G+* level for DEST cation in the gas phase.

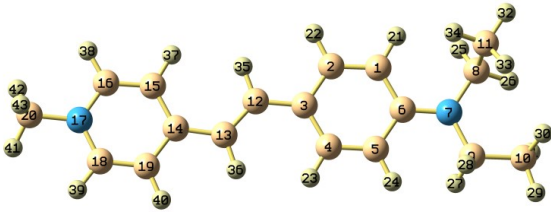
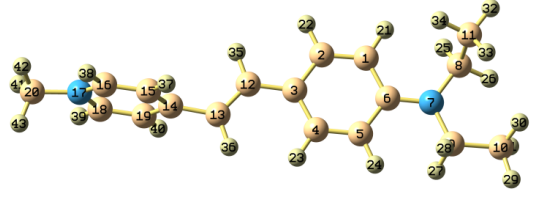
<i>Optimized S_0</i>							
							
Ethylenic C=C	Quinoidal C=C in pyridyl group		Quinoidal C=C in phenyl group		Dihedrals		
$C_{12}-C_{13}$ (Å)	$C_{15}-C_{16}$ (Å)	$C_{18}-C_{19}$ (Å)	C_1-C_2 (Å)	C_4-C_5 (Å)	$C_{12}-C_{13}-C_{14}-C_{15}$ (°)	$C_2-C_3-C_{12}-C_{13}$ (°)	$C_1-C_6-N_7-C_9$ (°)
1.37	1.36	1.37	1.37	1.37	0.37	179.71	176.06
<i>Optimized S_1</i>							
							
Ethylenic C=C	Quinoidal C=C in pyridyl group		Quinoidal C=C in phenyl group		Dihedrals		
$C_{12}-C_{13}$ (Å)	$C_{15}-C_{16}$ (Å)	$C_{18}-C_{19}$ (Å)	C_1-C_2 (Å)	C_4-C_5 (Å)	$C_{12}-C_{13}-C_{14}-C_{15}$ (°)	$C_2-C_3-C_{12}-C_{13}$ (°)	$C_1-C_6-N_7-C_9$ (°)
1.36	1.36	1.36	1.36	1.36	-91.61	-179.75	-176.62

Table ST3: Vibrational frequencies of the optimized S_0 in the C=C stretching region in CAM-B3LYP/6-31+G* level in of DEST in the gas phase.

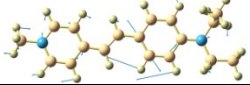
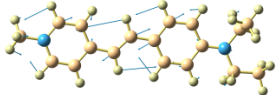
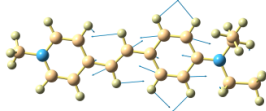
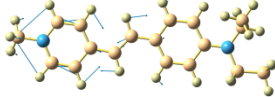
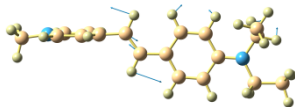
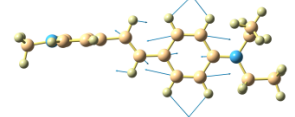
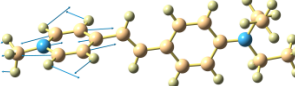
S_0 frequencies (cm^{-1})			
Unscaled (IR, Raman activity)	Scaled by 0.97	Raman frequencies from experiment in methanol	Mode description
1605 (IR 22, R 550)	1557	1551	Ring C=C, C-C and C-N asymmetric stretching coupled with in-plane wagging 
1633 (IR 2784, R 7698)	1584	1584	Ethylenic C=C stretching coupled with ring C-H in-plane wagging 
1708 (IR 62, R 222)	1657	1623	Ethylenic C=C stretching coupled with donor ring C=C stretching 
1738 (IR 154, R 193)	1686	-	Ethylenic C=C stretching coupled with acceptor ring C=C stretching 

Table ST4: Vibrational frequencies of the optimized S_1 in the C=C stretching region in CAM-B3LYP/6-31+G* level in of DEST in the gas phase.

S_1 Frequencies (cm^{-1})	
Unscaled	Mode description
1610	Ethylenic C=C stretching coupled with ring bending 
1698	Ethylenic C=C stretching coupled with donor C=C stretching 
1743	Acceptor C=C stretching 

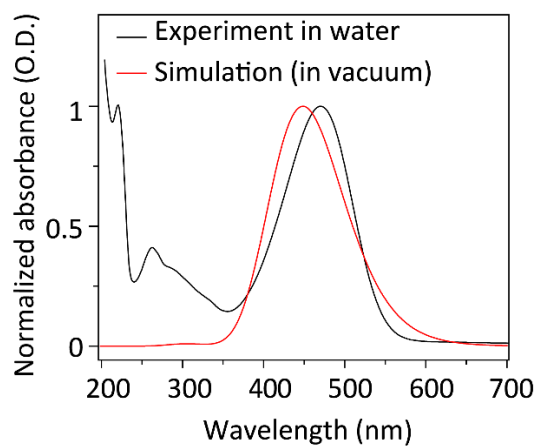
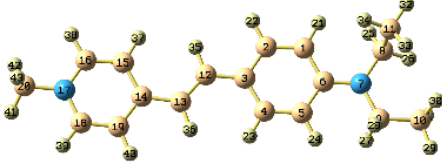
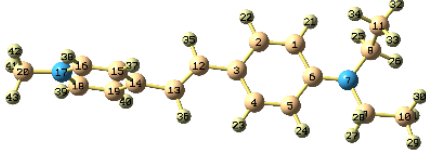
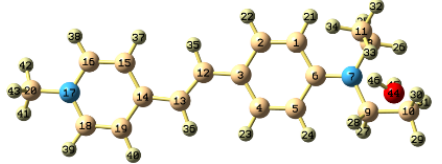
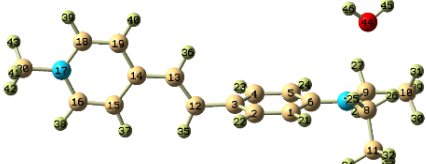
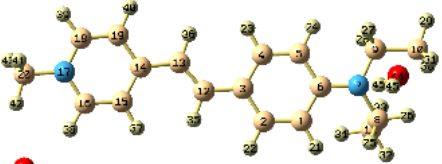
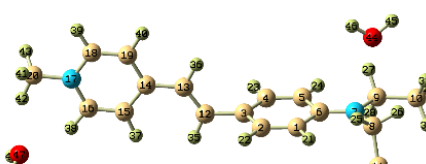


Figure S8: Comparison between calculated transition energies and intensities (at the CAM-B3LYP/6-31+G* level, in a vacuum) and absorption spectrum of DEST in water.

Table ST5: Calculated dipole moments of the DEST cation in the ground and excited states in the DFT/CAM-B3LYP/6-31+G (d) level of theory.

Type of calculation	S ₀ Structure with dipole moment (Debye)	S ₁ Structure with dipole moment (Debye)
Vacuum/ Gas phase	 <p>11.28</p>	 <p>6.47</p>
1:1 DEST: water located near N,N-diethyl amine group, in vacuum	 <p>15.25</p>	 <p>5.97</p>
1:2 DEST: water, in vacuum	 <p>16.72</p>	 <p>6.35</p>

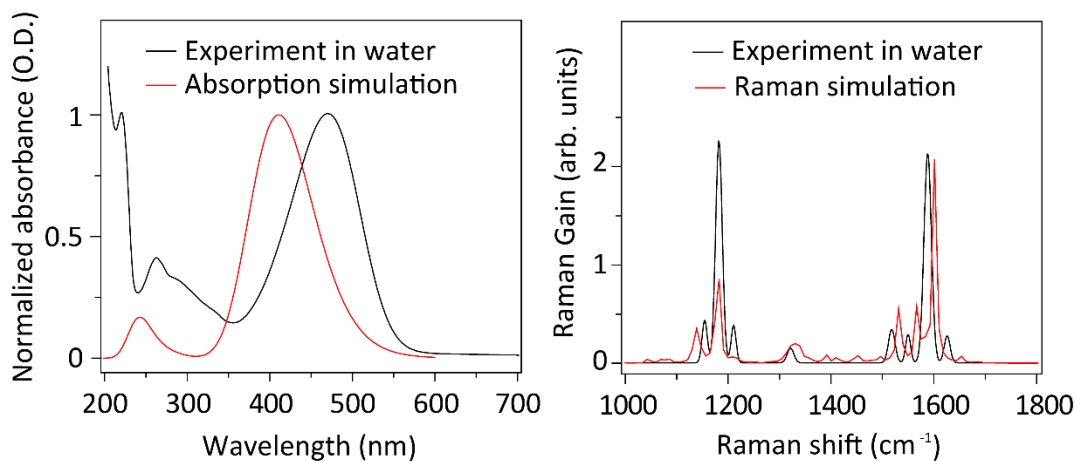
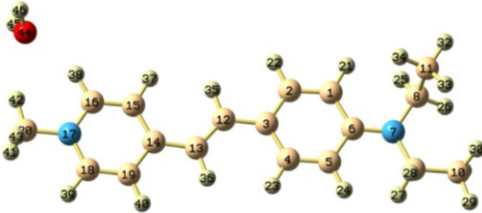
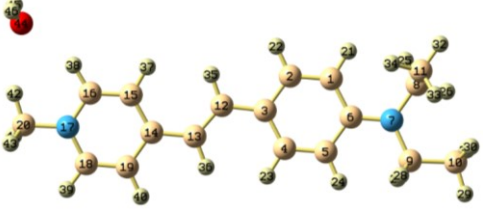


Figure S9: Comparison between experimental and simulated spectra at the CAM-B3LYP/6-31+G* level, vacuum calculation, with a water molecule near the pyridyl nitrogen (for optimized geometry see the following table ST9). The agreement between Raman frequencies and relative intensities has improved substantially from the gas phase calculation (c.f. Figure S6). Although the prediction of vertical transition intensities is better compared to the gas phase calculation, the match between transition frequencies is worse.

Table ST6: Structural parameters of the optimized S_0 and S_1 in CAM-B3LYP/6-31G+* level for DEST cation with a water molecule near the pyridyl N.

<i>Optimized S_0</i>							
							
Ethylenic C=C	Quinoidal C=C in pyridyl group		Quinoidal C=C in phenyl group		Dihedrals		
C ₁₂ -C ₁₃ (Å)	C ₁₅ -C ₁₆ (Å)	C ₁₈ -C ₁₉ (Å)	C ₁ -C ₂ (Å)	C ₄ -C ₅ (Å)	C ₁₂ -C ₁₃ -C ₁₄ -C ₁₅ (°)	C ₂ -C ₃ -C ₁₂ -C ₁₃ (°)	C ₁ -C ₆ -N ₇ -C ₉ (°)
1.36	1.37	1.37	1.37	1.37	-0.67	179.02	175.72
<i>Optimized S_1</i>							
							
Ethylenic C=C	Quinoidal C=C in pyridyl group		Quinoidal C=C in phenyl group		Dihedrals		
C ₁₂ -C ₁₃ (Å)	C ₁₅ -C ₁₆ (Å)	C ₁₈ -C ₁₉ (Å)	C ₁ -C ₂ (Å)	C ₄ -C ₅ (Å)	C ₁₂ -C ₁₃ -C ₁₄ -C ₁₅ (°)	C ₂ -C ₃ -C ₁₂ -C ₁₃ (°)	C ₁ -C ₆ -N ₇ -C ₉ (°)
1.37	1.37	1.37	1.37	1.37	-1.84	175.29	176.86

This model clearly shows that screening of charge does not lead to TICT model. A different

starting geometry with a Hydrogen bonded water molecule to the acceptor group is used in the following sections to see whether an initially H- bonded model may lead to a TICT geometry.

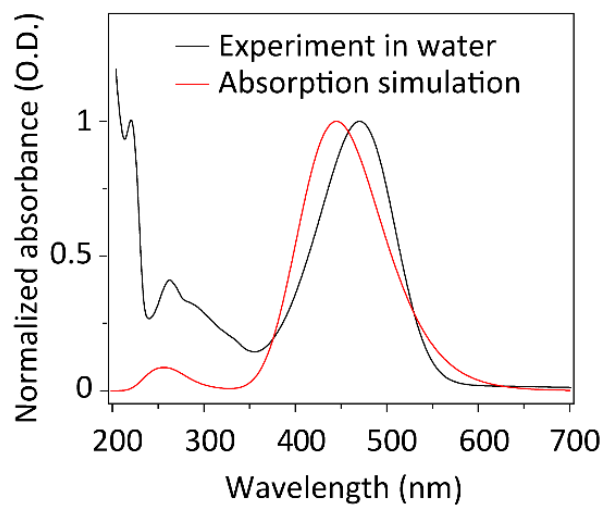
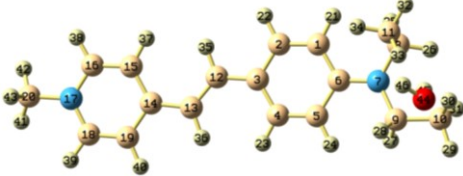
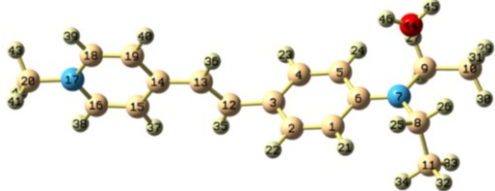


Figure S10: Comparison between experimental absorption spectrum of DEST in water and simulated spectra at the CAM-B3LYP/6-31+G* level, vacuum calculation, with a water molecule near the amine group N of the donor (for optimized geometry see the following table ST7).

Table ST7: Structural parameters of the optimized S_0 and S_1 in CAM-B3LYP/6-31G+* level for DEST cation with a water molecule near the amine N of the donor group.

<i>Optimized S_0</i>							
							
Ethylenic C=C	Quinoidal C=C in pyridyl group		Quinoidal C=C in phenyl group		Dihedrals		
C ₁₂ -C ₁₃ (Å)	C ₁₅ -C ₁₆ (Å)	C ₁₈ -C ₁₉ (Å)	C ₁ -C ₂ (Å)	C ₄ -C ₅ (Å)	C ₁₂ -C ₁₃ -C ₁₄ -C ₁₅ (°)	C ₂ -C ₃ -C ₁₂ -C ₁₃ (°)	C ₁ -C ₆ -N ₇ -C ₉ (°)
1.36	1.37	1.37	1.37	1.37	-0.64	179.48	171.12
<i>Optimized S_1</i>							
							
Ethylenic C=C	Quinoidal C=C in pyridyl group		Quinoidal C=C in phenyl group		Dihedrals		
C ₁₂ -C ₁₃ (Å)	C ₁₅ -C ₁₆ (Å)	C ₁₈ -C ₁₉ (Å)	C ₁ -C ₂ (Å)	C ₄ -C ₅ (Å)	C ₁₂ -C ₁₃ -C ₁₄ -C ₁₅ (°)	C ₂ -C ₃ -C ₁₂ -C ₁₃ (°)	C ₁ -C ₆ -N ₇ -C ₉ (°)
1.36	1.36	1.36	1.37	1.37	0.06	90.32	176.99

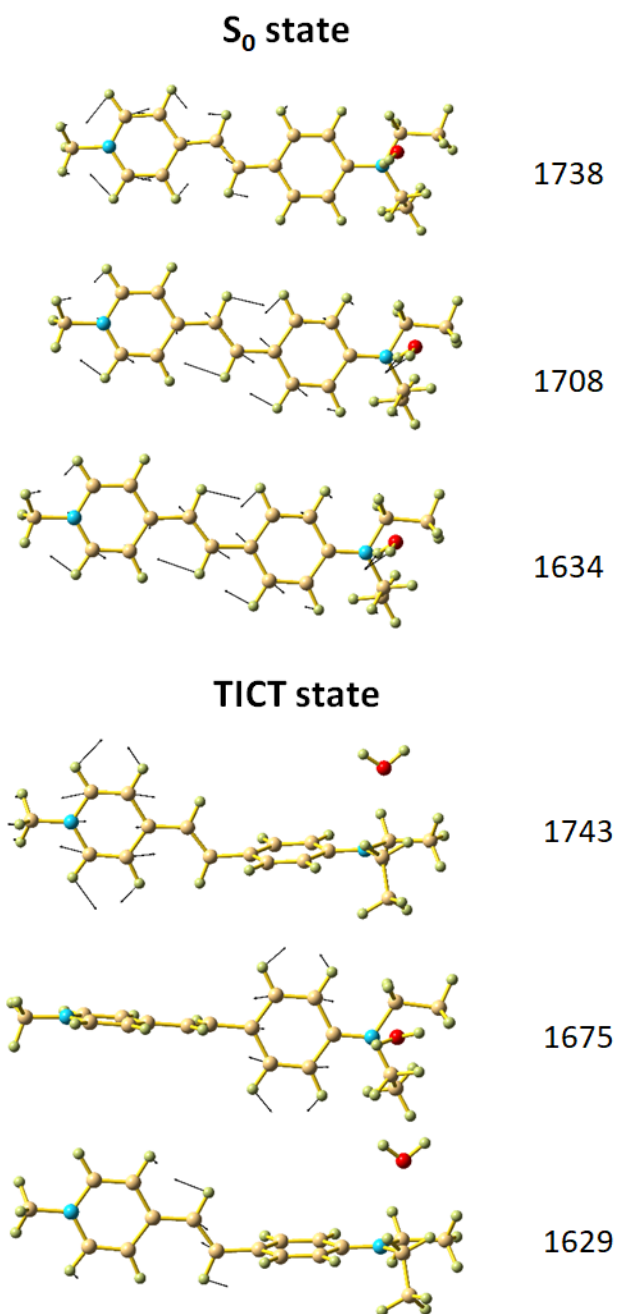


Figure S11a: Normal mode description of C=C stretching modes in the ground and TICT states of the 1:1 DEST-water complex described in Table ST7 and calculated in vacuum at the CAM-B3LYP/6-31+G* level..

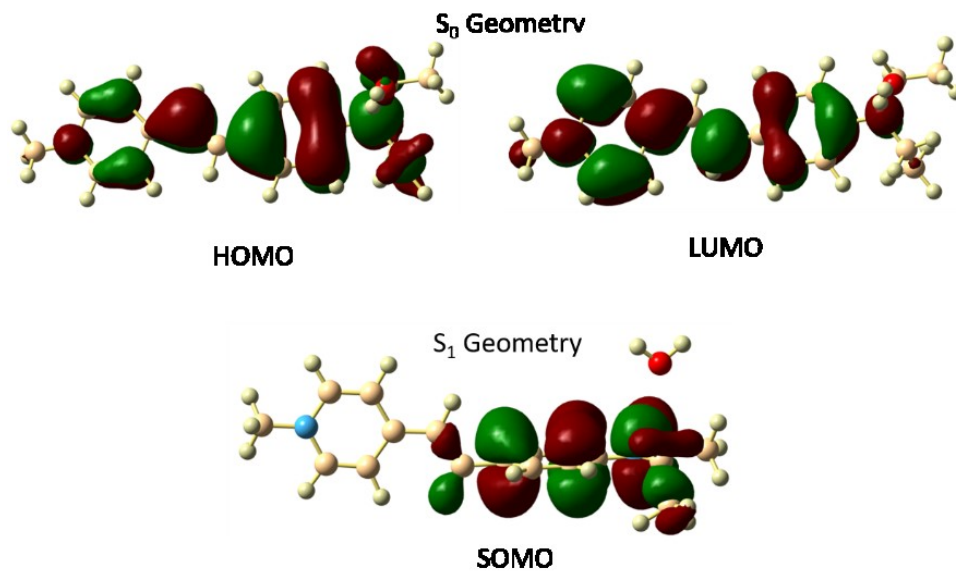


Figure S11b: MO diagrams showing the flow of charge during vertical excitation and TICT formation with a single water molecule near the amine group in the CAM-B3LYP/6-31+G* level, vacuum calculation.

The above model shows a TICT state, but in contrast to the gas phase model, the twist is now in the donor group, i.e. along $C_2-C_3-C_{12}-C_{13}$ dihedral. The calculated vibrational modes in the excited state for this model are compared with FSRS data for this model in the main manuscript (Figure 4).

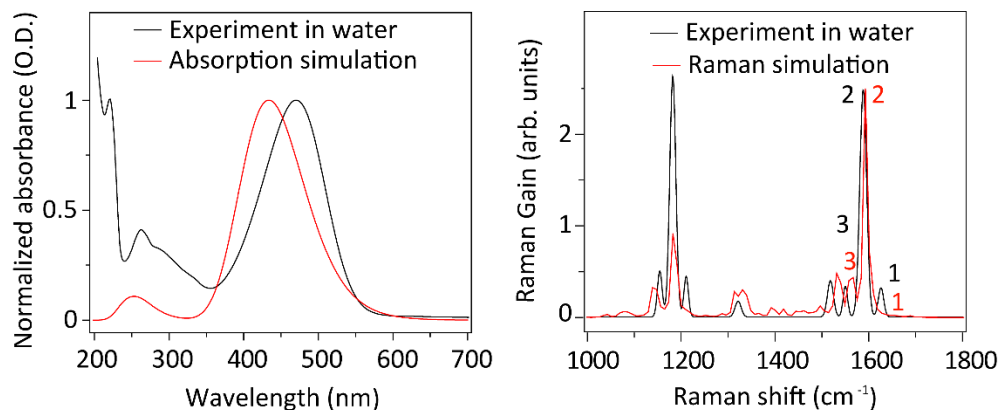
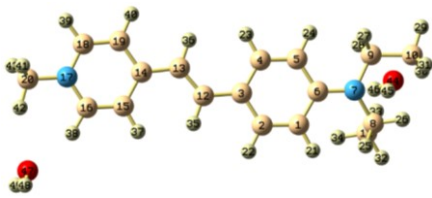
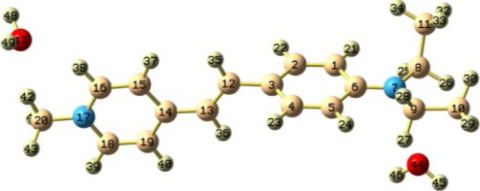


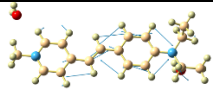
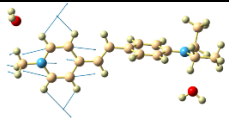
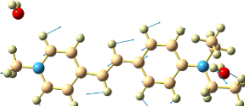
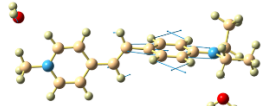
Figure S12: Comparison between experimental and simulated spectra at the CAM-B3LYP/6-31+G* level, vacuum calculation, with two water molecules: one near the amine group N of the donor and the other water molecule near the acceptor pyridinium group N (for optimized geometry see the following table ST8). The agreement between Raman frequencies and relative intensities are reasonable for this model as well. Vertical transition intensities for absorption are a good match, but transition frequencies are slightly more red-shifted than the previous model (Figure S10).

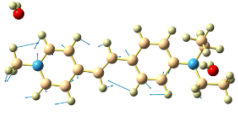
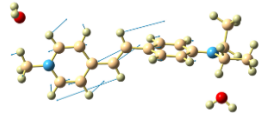
Table ST8: Structural parameters of the optimized S_0 and S_1 in CAM-B3LYP/6-31G+* level in the gas phase for DEST cation with two water molecules near DEST.

<i>Optimized S_0</i>							
							
Ethylenic C=C	Quinoidal C=C in pyridyl group		Quinoidal C=C in phenyl group		Dihedrals		
C ₁₂ -C ₁₃ (Å)	C ₁₅ -C ₁₆ (Å)	C ₁₈ -C ₁₉ (Å)	C ₁ -C ₂ (Å)	C ₄ -C ₅ (Å)	C ₁₂ -C ₁₃ -C ₁₄ -C ₁₅ (°)	C ₂ -C ₃ -C ₁₂ -C ₁₃ (°)	C ₁ -C ₆ -N ₇ -C ₉ (°)
1.36	1.37	1.37	1.38	1.38	-0.38	179.66	170.76
<i>Optimized S_1</i>							
							
Ethylenic C=C	Quinoidal C=C in pyridyl group		Quinoidal C=C in phenyl group		Dihedrals		
C ₁₂ -C ₁₃ (Å)	C ₁₅ -C ₁₆ (Å)	C ₁₈ -C ₁₉ (Å)	C ₁ -C ₂ (Å)	C ₄ -C ₅ (Å)	C ₁₂ -C ₁₃ -C ₁₄ -C ₁₅ (°)	C ₂ -C ₃ -C ₁₂ -C ₁₃ (°)	C ₁ -C ₆ -N ₇ -C ₉ (°)
1.37	1.36	1.36	1.37	1.37	-0.14	90.16	177.06

This model too predicts a TICT state with respect to rotation about the C₂-C₃-C₁₂-C₁₃ dihedral. The charge solvation by the water near pyridinic N does not override the effect of the H-bonding water near the amine group. This demonstrates that a H-bonding interaction in the starting geometry is more influential in the formation of TICT state compared to the stabilization of charge and dipole in DEST. The calculated vibrational modes in the excited state for this model shown in the following table (Table ST9) are very similar to that in the single H-bonded water model.

Table ST9: Raman vibrational frequencies in the S₀ using DFT/CAM-B3LYP/6-31+G* level and normal modes with IR intensities computed in the S₁ in the TD-DFT/CAM-B3LYP/6-31+G* level of DEST cation with two water molecules in the gas phase.

S ₀ Frequencies (cm ⁻¹)			S ₁ Frequencies (cm ⁻¹)		
Mode no.	Calculated value (scaled by 0.97), experimental value	Mode description	Mode no.	Calculated value, experimental value	Mode description
1	1708 (1657), 1625	 Coupled ring and bridge C=C stretching	1'	1743, 1650	 Isolated ring C=C stretching
2	1642 (1593), 1584	 Coupled ring and bridge C=C stretching and C-H bending	2'	1675, 1577	 Coupled ring C=C stretching and C-H bending

3	1611 (1562), 1577		3'	1626, 1518	
		Coupled C=C asymmetric stretching and C-h bending			Coupled ring and bridge C=C stretching and C-H bending

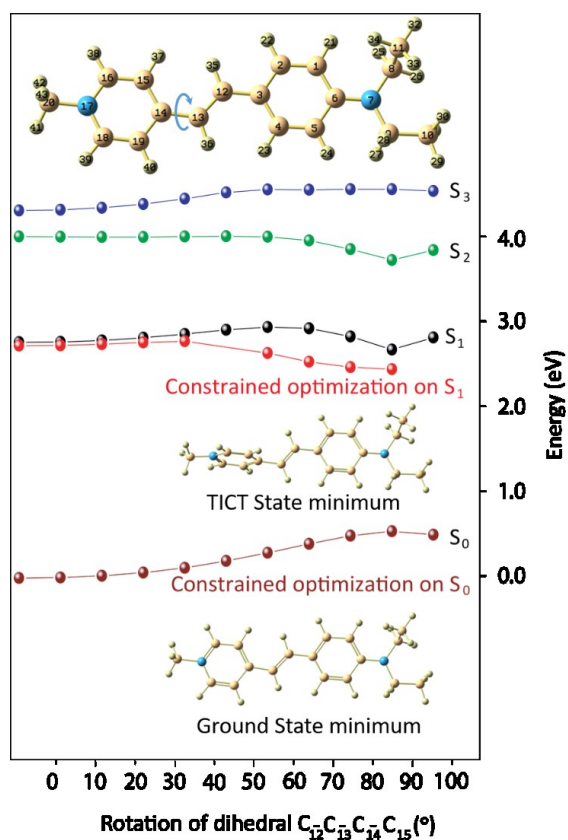


Figure S13: Constrained gas-phase DFT/TDDFT optimization scans of the twist (rotation of $C_{12}-C_{13}-C_{14}-C_{15}$ dihedral) on S_0 and S_1 excited state surfaces of the DEST cation in the gas phase. The dihedral is chosen according to the optimized S_1 structure described in Table ST2. A shallow local minimum on the S_1 surface (shown by red dots and lines) is observed, and the barrier for TICT formation is small, ~ 0.05

eV, while TICT structure (with the acceptor ring perpendicular to the molecular plane) is the global minimum. TDDFT vertical excitation energies (shown with black dots and lines) from the constrained optimized geometries on the S_0 surface (constructed with respect to torsion about the same dihedral) confirm the small barrier for TICT state relaxation. These scans also show energetically well-separated (> 0.3 eV) S_1 , S_2 and S_3 surfaces indicating that the TICT relaxation involves only one excited state (S_1) surface.

References

1. Dharmadhikari, A. K.; Sandhu, A. S.; Dharmadhikari, J. A.; Mishra, A.; Kumar, G. R. Measurement of two-photon absorption cross-section in organic molecular salt with linear and circular polarized radiation. *Appl. Phys. B* **2004**, *79*, 235-238.
2. Jha, A.; Chakraborty, D.; Srinivasan, V.; Dasgupta, J. Photoinduced Charge Transfer in Solvated Anthraquinones Is Facilitated by Low-Frequency Ring Deformations. *J.Phys.Chem. B* **2013**, *117*, 12276-1228.
3. Roy, P.; Karmakar, S.; Dasgupta, J. Femtosecond Stimulated Raman Spectroscopy. *Molecular and Laser Spectroscopy*; **2017**, Chapter 9, 1st ed.; Elsevier.
5. Gaussian 09, Revision A.1, Frisch; M. J. *et al.* Gaussian, Inc., Wallingford CT, **2009**.
4. Roy, P.; Jha, A.; Yasarapudi, V. B.; Ram, T.; Puttaraju, B.; Patil, S.; Dasgupta, J. Ultrafast bridge planarization in donor- π -acceptor copolymers drives intramolecular charge transfer. *Nat. Commun.* **2017**, *8*, 1716.
6. Furniss, B. S., Hannaford, A.J., Smith, P.W.G. & Tatchell, A.R. Vogel's textbook of practical Organic Chemistry, 5th ed. **1988**, John Wiley & Sons: New York.
7. Lange's Handbook of Chemistry, Seventeenth Edition Publisher: McGraw-Hill Education **2017**.
8. Cheeseman, J.R.; Frisch, M.J. Basis set dependence of vibrational Raman and Raman optical activity intensities. *J. Chem. Theory Comput.* **2011**, *7(10)*, 3323-3334.
9. Jiménez-Hoyos, C. A.; Janesko, B. G.; Scuseria, G. E. Evaluation of range-separated hybrid density functionals for the prediction of vibrational frequencies, infrared intensities, and Raman activities. *Phys. Chem. Chem. Phys.* **2008**, *10(44)*, 6621-6629.
10. Yanai, T.; Tew, D. P.; Handy, N. C A new hybrid exchange-correlation functional using the Coulomb-attenuating method (CAM-B3LYP). *Chem. Phys. Lett.* **2004**, *393*, 51-57.

11. Foster, M. E.; Sohlberg, K. Empirically corrected DFT and semi-empirical methods for non-bonding interactions. *Phys. Chem. Chem. Phys.* **2010**, *12*(2), 307-322.